

폴리프로필렌/점토 나노복합체의 하이브리드 나노구조에 따른 기계적 성질 및 결정화거동 변화

최기운 · 이한섭 · 강복춘 · 양회창[†]

인하대학교 나노시스템공학부 섬유신소재공학과

(2009년 12월 21일 접수, 2010년 2월 18일 수정, 2010년 2월 27일 채택)

Hybrid Nanostructure-dependent Mechanical Properties and Crystallization Behaviors of Polypropylene/Clay Nanocomposites

Kiwoon Choi, Han Sup Lee, Bok Choong Kang, and Hoichang Yang[†]

Department of Advanced Fiber Engineering, Inha University,

253 Yonghyun-dong, Nam-gu, Incheon 402-751, Korea

(Received December 21, 2009; Revised February 18, 2010; Accepted February 27, 2010)

초록: 아미노실란 처리된 점토를 제조하여, 이를 분자량이 서로 다른 폴리프로필렌(140 kg/mol과 410 kg/mol)과 상용화제인 무수말레인산 그래프트 폴리프로필렌(50 kg/mol)과 함께 170 °C 및 190 °C에서 용융혼합법으로 각각의 폴리프로필렌/점토 나노복합체를 제조하였다. 무수말레인산 그래프트 폴리프로필렌과 용융혼합과정에서 낮은 분자량의 폴리프로필렌은 점토 층 사이로 쉽게 침투하여 층간 거리를 58 Å 이상으로 증가시키지만, 첨가된 점토는 60~80 nm 두께의 응집체로 나노복합체 내에 분산상을 이룬다. 이와 달리 높은 분자량의 폴리프로필렌 기반 나노복합체에서는 점토는 27 Å로 낮은 박리 정도를 보이며, 전반적으로 고른 점토 분산상을 형성한다. 분자량 및 용융혼합공정의 차이에 따른 폴리프로필렌/점토 나노복합체의 미세 모풀로지 차이로 기계적 물성 및 결정화거동이 관찰되었으며, 분자량 410(kg/mol)인 폴리프로필렌은 개질된 점토를 1~3 wt% 첨가함으로써 순수 폴리프로필렌의 연성특성을 유지하면서 향상된 인장강도와 탄성률을 보였다.

Abstract: Clay-loaded polypropylene (PP) nanocomposites were fabricated via melt-compounding of two molecular weight (M_w) PPs (140 and 410 kg/mol) and octadecylamine-treated clay (C18MMT), with the assistance of maleic anhydride-grafted PP(PP-MAH), respectively, at 170 °C and 190 °C. At both melt-compounding temperatures, the low- M_w PP tends to easily diffuse into silicate layers, especially in the presence of the mobile PP-MAH, resulting in a marked increase in silicate layer spacing (above 58 Å), when compared to 27 Å in the high- M_w PP-based system. Due to relatively lower melt-viscosity of the low- M_w PP-based system, however, there existed quasi-stacked clay aggregates with a thickness of 60~80 nm, while the high- M_w PP-based nanocomposites showed relatively homogeneous dispersion of clays. The different morphologies are mainly related to changes in the viscoelastic properties of PPs, dependent on the processing temperature and their M_w s. The slight differences in nanocomposites induce discernible crystallization and mechanical behaviors. High- M_w PP-based nanocomposites containing 1~3 wt% C18MMT showed improvement in both tensile strength and modulus, while maintaining the inherent ductility of pure PP.

Keywords: polypropylene, nanocomposite, clay, toughening, crystallization.

Introduction

Polymer/clay nanocomposites show dramatic enhancements in mechanical, thermal, and gas barrier properties with relative low loading, when compared to conventional fillers.^{1~6} Montmorillonite (MMT) is one of several types of mineral-based clays that can be natural or synthetic magnesium

aluminum silicate with each individual hydrophilic platelets.^{7,8} Numerous studies of polymer/clay nanocomposite fabrication have reported that ion-exchangeable organo-alkyl molecules or additional polymers with polar components should be incorporated to enhance an intercalated structure or exfoliation state of clays in the polymer matrix.^{9,10} Polymer/clay nanocomposites are generally prepared by solution-blending or melt-compounding a polymer with an ion-exchanged organoclay,¹⁰ and then by *in-situ* polymerization under clay sus-

[†]To whom correspondence should be addressed.
E-mail: hcyang@inha.ac.kr

pension.^{2,4,11} Among the methods of incorporating organo-clay into host polymers, melt-compounding has appeal for fabricating polymer/clay nanocomposites due to its potential for large scale polymer processing.

This paper reports on investigations of host polymer molecular weight (M_w) effects on hybrid nanostructure formation of polypropylene (PP)/clay nanocomposites during melt-compounding, operated at different temperatures. In this study we also correlated the hybrid nanostructures with the corresponding crystallization behaviors and tensile properties. Since a hydrophobic PP does not provide a good affinity with pristine or ion-exchanged clays, the nanoscale dissociation of layered silicates in the PP matrix itself has not been realized. However, the clay dispersion is significantly improved by incorporating a polyolefin derivative with a polar moiety, e.g., maleic anhydride-grafted PP (PP-MAH). By compounding octadecylamine-treated clay (C18MMT), PP-MAH and PP at the same time, the Toyota group reported that the loading of PP-MAH significantly improved the dispersion of inorganic clays in the PP matrix, resulting in high performance of mechanical properties.¹⁰ Hasegawa *et al.* also reported that the silicate layer distance increased with an increase in PP-MAH content, and that its large-scale extension is highly linked to mechanical properties of PP/PP-MAH/clay nanocomposites.⁹

For semi-crystalline polymer nanocomposites, the confined geometry aspects of dispersed nanofillers significantly affect crystal nucleation and growth of the polymer matrix.¹²⁻¹⁷ However, most works have been focused on either mechanical properties or crystallization behaviors of semi-crystalline polymer/clay nanocomposites, depending on the chain confinement by loaded fillers. We have systematically investigated morphologies, crystallization behaviors, and tensile properties of melt-compounded PP/clay nanocomposites. The PP nanocomposites used in this study were prepared via melt-compounding C18MMT, PP-MAH ($M_w=50$ kg/mol) and PPs with different M_w s (140 and 410 kg/mol), respectively. Characterization of the nanocomposites was performed by transmission electron microscopy (TEM), differential scanning calorimetry (DSC), X-ray diffraction (XRD), and tensile analysis.

Experimental

Materials and Sample Preparation. PPs and PP-MAH ($M_w=50$ K, kg/mol, MAH content ~5 wt%) were provided from Daelim Co. ($M_w=410$ K), Korea Petrochemical Ind. Co. ($M_w=140$ K), and Honam Petrochemical Co, respectively. MMT (Kunimine Co.) as a clay was treated with octadecylamine (Aldrich), as described in literature.¹ In the C18MMT organo-

clay, the ratio of MMT to octadecylamine (ODA) was fixed at approximately 8:3 in weight. PPs, PP-MAH, and C18MMT were completely dried in a vacuum oven held at 80 °C, and then were physically mixed together. Melt-compounding was performed at either 170 °C or 190 °C for 10 min, using an internal mixer (Brabender) with a twin screw. The C18MMT content varied from 1–7 wt% in the PP nanocomposites, and the ratio of C18MMT to PP-MAH was fixed at 1:3, the expected optimum ratio to obtain the nanocomposites.¹⁰ The melt-compounded samples were compression-molded at 190 °C and cooled down to room temperature at a rate of 10 °C/min. Finally, they were machine-cut with a dumbbell shape (width × thickness × length, 4.7 mm × 3.13 mm × 20 mm).

Characterization. The interlayer spacing, $d_{(001)}$ of silicate platelets in pristine MMT was compared with those in C18MMT, PP/C18MMT, and PP/PP-MAH/C18MMT nanocomposites, as calculated from XRD (Rigaku diffractometer) profiles. DSC (DSC7, Perkin Elmer) was performed to monitor non-isothermal crystallization behaviors of the nanocomposites. In this case, a 5–6 mg sample was completely melted at 200 °C for 10 min, and then non-isothermally crystallized with a cooling rate of 10 °C/min. Overall morphologies and clay dispersion in the PP nanocomposites were observed using TEM (1200EX, JEOL), operating at 120 kV. The samples were sectioned to a film thicknesses of about 50 nm using a cryogenic ultramicrotome system (MT-XL, Boeckeler Instruments, Inc) with a diamond knife (DiATOME) at -20 °C. Then, the sectioned films were collected on 300-mesh copper grids. The tensile properties of PP/PP-MAH/C18MMT nanocomposites measured using a universal testing machine (Instron 4026), operating at a crosshead speed of 5 mm/min, were compared with those of control PP/PP-MAH blends.

Results and Discussion

Hybrid Nanostructures. Figure 1 represents typical XRD profiles showing discernible changes in $d_{(001)}$ within C18MMT and PP/C18MMT nanocomposites, and schemes of the corresponding hybrid structures. Table 1 represents the XRD peak positions and the $d_{(001)}$ values from the silicate layers. After the ODA treatment for MMT, values of $d_{(001)}$ are dramatically increased from 9.90 to 24.1 Å, as calculated by peak positions in XRD profiles, due to the favorable diffusion of amphiphilic ODA into the pristine MMT. Unlike the oligomer compatible with the clay, the additional diffusion of hydrophobic PP supramolecules into C18MMT is only improved in the presence of hydrophilic PP-MAH, as determined by the X-ray peak shift to lower angle (Figure 1): values of $d_{(001)}$ in the PP/C18MMT (90/10) and PP/PP-

MAH/C18MMT (60/30/10) nanocomposites are 30.9 Å and 35.9 Å, respectively.

Based on the results, hybrid nanostructures in PP/PP-MAH/clay nanocomposites were further controlled via melt-compounding PPs ($M_w=140$ K and 410 K), PP-MAH, and C18MMT, with different blending ratios, at two mixing temperatures of 170 °C and 190 °C. Figure 2 represents XRD profiles of PP/PP-MAH/C18MMT nanocomposites melt-compounded at 170 °C. For the low- M_w PP (140 K) based nanocomposites containing 1–7 wt% C18MMT loadings, there exists no clear X-ray reflection from ordered silicate layers (Figure 2(a)). The results expect that the silicate platelets are well dissociated above the upper limitation of XRD (58 Å) used in this study. However, the high- M_w PP based nanocomposites still show broad X-ray reflections around $2\theta=3.3^\circ$, corresponding to $d_{(001)} \sim 26.7$ Å. The peak intensities slightly increase with the C18MMT content. The different dissociation of clay in the PP matrices is mainly related to the chain length of PP: the steric volume of PP increases with an increase in the chain length,¹⁸ preventing the diffusion of the high- M_w PP into intercalated clay layers.

Unlike XRD providing the degree of the clay dissociation, TEM analysis provides detailed information for both local

and overall dispersion of the clay in the PP matrices. Therefore, the combined characterizations for polymer/clay nanocomposites have the advantage of the correlation between hybrid nanostructures and macroscopic properties, such as mechanical, gas barrier properties, and flame retardance.^{19–23} Figure 3 displays typical TEM micrographs of 3 wt% C18MMT/PP nanocomposites melt-compounded at 170 °C. In the 140 K PP-based samples, silicate platelets form quasi-stacked aggregates with a lateral thickness of about 60 nm (Figure 3(a)), but each silicate layer is exfoliated above 80.0 Å (Figure 3(b)),

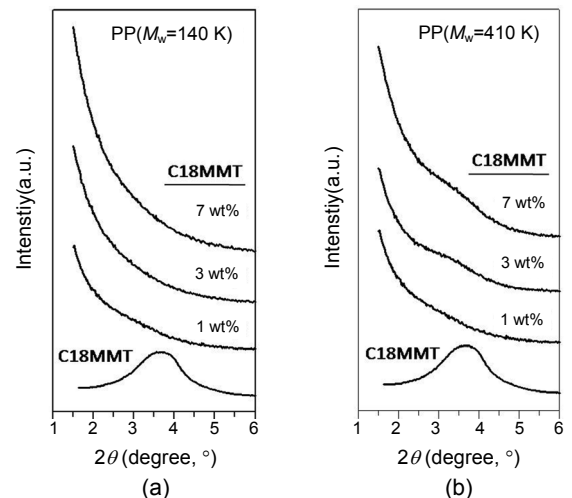


Figure 2. XRD profiles of PP/PP-MAH/clay nanocomposites with different C18MMT loadings: (a) PP, $M_w=140$ kg/mol and (b) PP, $M_w=410$ kg/mol.

Table 1. Typical Changes in the Intercalated Layer Spacing, $d_{(001)}$ of Clays

Designation	$2\theta(^{\circ})$	$d_{(001)}$
MMT	8.90	9.90 Å
C18MMT	3.66	24.1 Å
PP/C18MMT (90/10)	2.86	30.9 Å
PP/PP-MAH/C18MMT (83/7/10)	2.46	31.9 Å

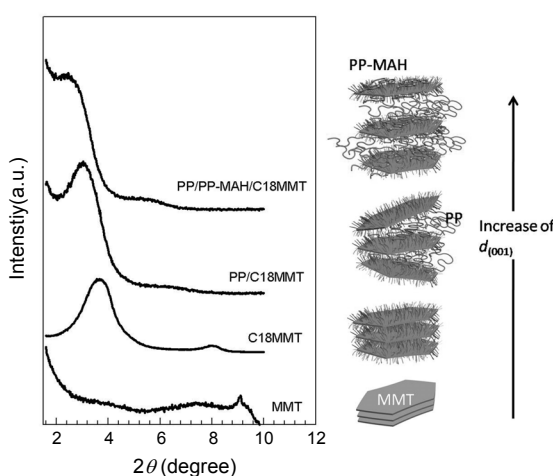


Figure 1. XRD profiles indicating different dissociation behaviors of the clay galleries by the incorporation of octadecylamine, PP, and PP-MAH (The right image represents schematic diagram showing changes in intercalated spacing, $d_{(001)}$ of the clay in MMT, C18MMT, PP/C18MMT, and PP/PP-MAH/C18MMT).

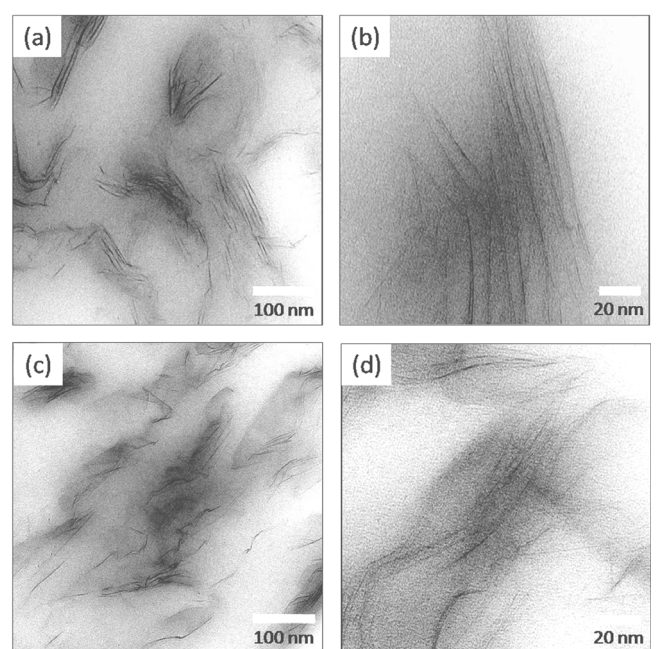


Figure 3. TEM micrographs of 3 wt% C18MMT-loaded PP/PP-MAH nanocomposites prepared at 170 °C: (a, b) PP, $M_w=140$ kg/mol; (c, d) PP, $M_w=410$ kg/mol.

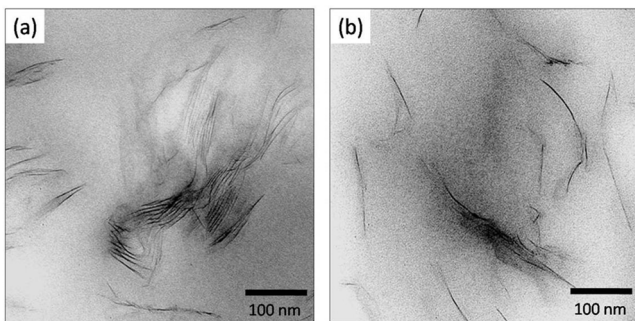


Figure 4. TEM micrographs of 3 wt% C18MMT-loaded PP/PP-MAH nanocomposites prepared at 190 °C: (a) PP, $M_w=140$ kg/mol; (b) PP, $M_w=410$ kg/mol.

which agrees with the XRD result. In the high- M_w PP matrix, however, they are well dispersed, although the silicate inter-spacing is not much expanded (Figure 3(c) and 3(d)). By comparing PP nanocomposites prepared at 170 °C and 190 °C, it is found that the clay dissociation is considerably improved in both different M_w PPs at a higher processing temperature, as determined in Figure 4.

The different morphologies are mainly related to changes in the viscoelastic properties of PPs, dependent on processing temperature and their M_w s. Like most semi-crystalline polymers, viscosities of PPs significantly decrease through crystal melting, especially if M_w is not enough high. It is expected that the 140 K PP matrix with a relatively low melt-viscosity does not provide enough shear force to individually separate silicate platelets.

Crystallization Behaviors of PPs in Confined Hybrid Geometries. In polymer nanocomposites, the crystal nucleation and growth of a semi-crystalline polymer are considerably affected by the confined geometries from loaded fillers. For C18MMT/PP/PP-MAH nanocomposites used in this study, the crystallization behaviors of the PPs were observed using DSC and compared with the controlled blends (with the same PP/PP-MAH ratios in the nanocomposites).

All samples kept at 200 °C for 10 min were melt-crystallized with a constant cooling rate of 10 °C/min. Figure 5 shows DSC cooling curves of PP nanocomposites with different C18MMT loadings and these control PP/PP-MAH blends melt-compounded at 170 °C. From the DSC curves, crystallization onset (T_{onset}) and peak (T_{peak}) temperatures of PPs were measured. For the control blends with the low- M_w PP, T_{peak} is shifted to a higher temperature from 111.6 to 112.8 °C with an increase in the PP-MAH content, while T_{peak} values for the high M_w -PP system are decreased from 119.0 to 117.9 °C. In addition, the changes in T_{onset} dependent on the PP matrices are similar to the trend in T_{peak} . The results suggest that PP-MAH co-crystallizes with the

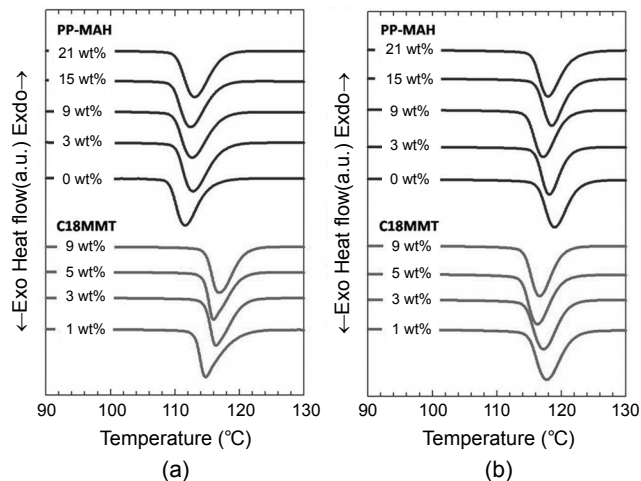


Figure 5. Non-isothermal cooling DCS curves of the control PP/PP-MAH blends and the corresponding PP/clay nanocomposites: (a) PP($M_w=140$ kg/mol); (b) PP($M_w=410$ kg/mol).

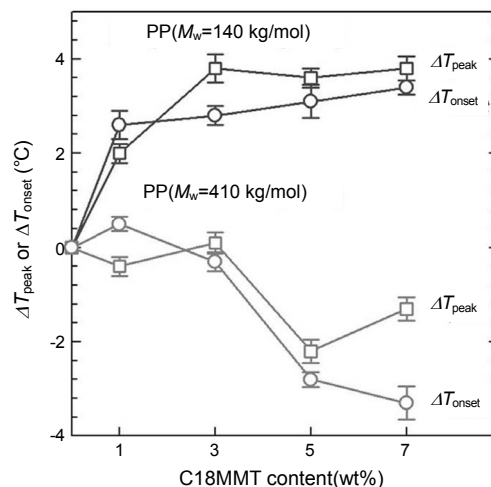


Figure 6. Variations in T_{onset} and T_{peak} of PP nanocomposites containing different C18MMT loadings.

low- M_w PP but it slightly interferes in the crystallization of the high- M_w PP.

It has been reported that PP and PP-MAH can either co-crystallize or phase-separate when they crystallize; a phase separation was observed in blends slowly crystallized with a cooling rate of 1 °C/min.²⁴⁻²⁷ In our study, there is no clear evidence of phase-separated PP domains in the both control blends, such as multiple exotherms or large shifts of T_{peak} , T_{on} to low temperature. It should be noted that small loadings of foreign fillers can reduce the free energy barrier to form a critical nucleus, or they can increase geometrical confinement to retard crystallization behavior of the matrix polymer.

Figure 6 represents temperature differences between the nanocomposites and the control blends, referred as to ΔT (= $T_{nanocomposite} - T_{blend}$), as a function of the C18MMT content

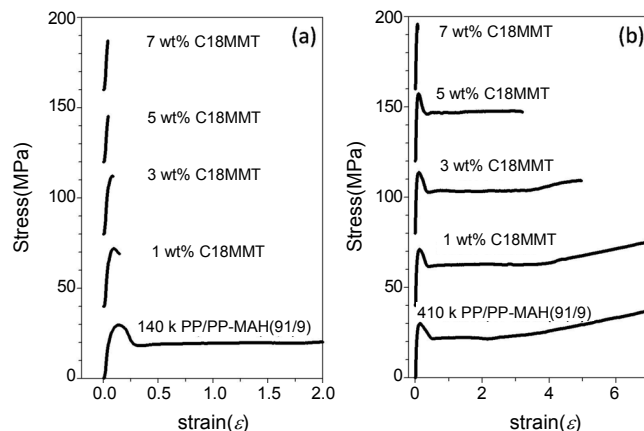


Figure 7. Typical stress–strain curves of control PP/PP–MAH blends and PP/PP–MAH/clay nanocomposites as a function of strain (ϵ): PP M_w =(a) 140 kg/mol; (b) 410 kg/mol (In all PP/clay nanocomposites, the ratio of C18MMT to PP–MAH was 1:3).

in the nanocomposites. For the low- M_w PP system, values of both ΔT_{peak} and ΔT_{onset} keep positive (black lines) and slightly increase with an increase in the clay content, while they show negative trend (grey lines) in the high- M_w PP system. The M_w -dependent crystallization behaviors of PPs are related to the hybrid nanostructures. As shown in Figure 3, the stacked clay aggregates in the low- M_w PP-based nanocomposites induce a less confined structure when compared to high- M_w PP systems. As a result, crystallization behavior of PP and PP–MAH in less confined geometries tends to follow the co-crystallization occurring in the control PP blends. In particular, heterogeneous clay surfaces act as nucleation sites for the PPs, resulting in positive values of ΔT_{peak} and ΔT_{onset} .

Tensile and Deformation Behaviors. The different hybrid nanostructures from the different PP matrices also affect mechanical properties of the clay/PP/PP–MAH nanocomposites. Tensile testing of dumbbell shaped specimens was performed using a universal testing machine operated with a strain (ϵ) rate of 25%/min, at room temperature. Figure 7 represents tensile stress–strain curves of different C18MMT-loaded PP/PP–MAH nanocomposites and control PP/PP–MAH (91/9) blends. From these stress–strain curves, tensile strengths and moduli for these samples were calculated (Figure 8). The control PP/PP–MAH blends containing up to 21 wt% PP–MAH show similar tensile strengths and elongations at break (above $\epsilon=7$), comparable to those of 140 K and 410 K PP homopolymers, although all data were not shown here.

For the nanocomposites, the incorporation of inorganic rigid clay tends to increase tensile strengths and moduli, although a decrease in tensile strength of the low- M_w PP systems

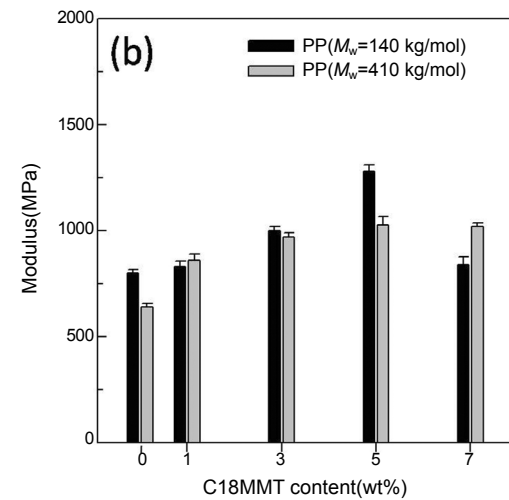
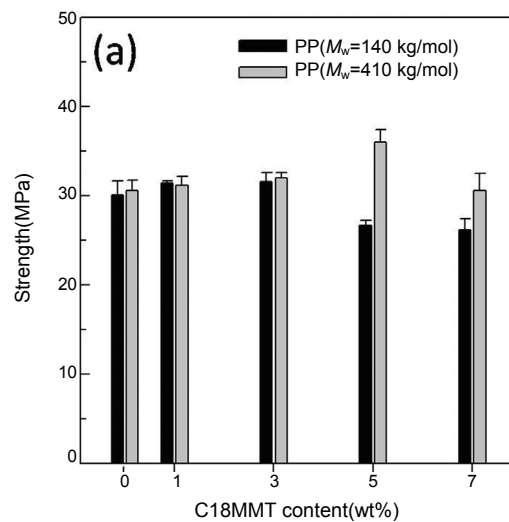


Figure 8. The tensile strengths (a); moduli (b) of PP/PP–MAH/clay nanocomposites prepared at 170 °C.

is indicated above 5 wt% C18MMT content. However, elongation at break of the nanocomposites suddenly drops with an increase in C18MMT content. In particular, low- M_w PP/clay nanocomposites become brittle and fail without any matrix deformation above 3 wt% C18MMT content. In contrast, the high- M_w PP-based nanocomposites still maintain ductile deformation behavior of PP, even with 5 wt% C18MMT. As a result, there are simultaneous enhancements in the tensile strength and modulus of the high- M_w PP systems, with a good elongation break comparable to that of pure PP.

Acknowledgment: This work was supported by the INHA UNIVERSITY Research Grant.

References

- Y. Kojima, A. Usuki, M. Kawasumi, A. Okada, Y. Fukushima,

1. T. Kurauchi, and O. Kamigaito, *J. Mater. Res.*, **8**, 1185 (1993).
2. J. Kim and S. Hwnag, *Polymer (Korea)*, **29**, 87 (2005).
3. M. Pramanik, S. K. Srivastava, B. K. Samantaray, and A. K. Bhowmick, *Macromol. Res.*, **11**, 260 (2003).
4. P. B. Messersmith and E. P. Giannelis, *J. Polym. Sci. Part A: Polym. Chem.*, **33**, 1047 (1995).
5. T. Lan, P. D. Kaviratna, and T. Pinnavaia, *J. Chem. Mater.*, **6**, 573 (1994).
6. A. Okada and A. Usuki, *Macromol. Mater. Eng.*, **291**, 1449 (2006).
7. U. Hoffman, K. Endell, and D. Z. Will, *Krist.*, **86**, 340 (1933).
8. T. J. Pinnavaia, *Science*, **220**, 365 (1983).
9. S. G. Lyu, E. Y. Park, K. S. Bae, and G. S. Sur, *Polymer (Korea)*, **25**, 421 (2001).
10. M. Kawasumi, N. Hasegawa, M. Kato, A. Usuki, and A. Okada, *Macromolecules*, **30**, 6333 (1997).
11. Y. Kojima, A. Usuki, M. Kawasumi, A. Okada, T. Kurauchi, and O. Kamigaito, *J. Polym. Sci. Part A: Polym. Chem.*, **31**, 983 (1993).
12. D. M. Lincoln, R. A. Vaia, and R. Krishnamoorti, *Macromolecules*, **37**, 4554 (2004).
13. D. M. Lincoln, R. A. Vaia, Z. G. Wang, and B. S. Hsiao, *Polymer*, **42**, 1621 (2001).
14. H. C. Yang, P. Bhimaraj, L. Yang, R. W. Siegel, and L. S. Schadler, *J. Polym. Sci. Part B: Polym. Phys.*, **45**, 747 (2007).
15. G. Turturro, G. R. Brown, and L. E. St Pierre, *Polymer*, **25**, 659 (1984).
16. S. H. Kim, S. H. Ahn, and T. Hirai, *Polymer*, **44**, 5625 (2003).
17. A. J. Waddon and Z. S. Petrovic, *Polym. J.*, **34**, 876 (2002).
18. E. Moncada, R. Quijada, and J. Retuert, *J. Appl. Polym. Sci.*, **103**, 698 (2007).
19. T. D. Fornes, P. J. Yoon, D. L. Hunter, H. Keskkula, and D. R. Paul, *Polymer*, **43**, 5915 (2002).
20. A. B. Morgan and J. W. Gilman, *J. Appl. Polym. Sci.*, **87**, 1329 (2003).
21. H. R. Dennis, D. L. Hunter, D. Chang, S. Kim, J. L. White, J. W. Cho, and D. R. Paul, *Polymer*, **42**, 9513 (2001).
22. A. Vermogen, K. Masenelli-Varlot, R. Seguela, J. Duchet-Rumeau, S. Boucard, and P. Prele, *Macromolecules*, **38**, 9661 (2005).
23. W. J. Boo, L. Sun, G. L. Warren, E. Moghbelli, H. Pham, A. Clearfield, and H. Sue, *J. Polymer*, **48**, 1075 (2007).
24. J. Duvall, C. Sellitti, C. Myers, A. Hiltner, and E. Baer, *J. Appl. Polym. Sci.*, **52**, 207 (1994).
25. J. Duvall, C. Sellitti, V. Topolkaraev, A. Hiltner, E. Baer, and C. Myers, *Polymer*, **35**, 3948 (1994).
26. J. Duvall, C. Sellitti, C. Myers, A. Hiltner, and E. Baer, *J. Appl. Polym. Sci.*, **52**, 195 (1994).
27. K. W. Cho, F. K. Li, and J. Choi, *Polymer*, **40**, 1719 (1999).